Journal of Materials Chemistry C

Accepted Manuscript

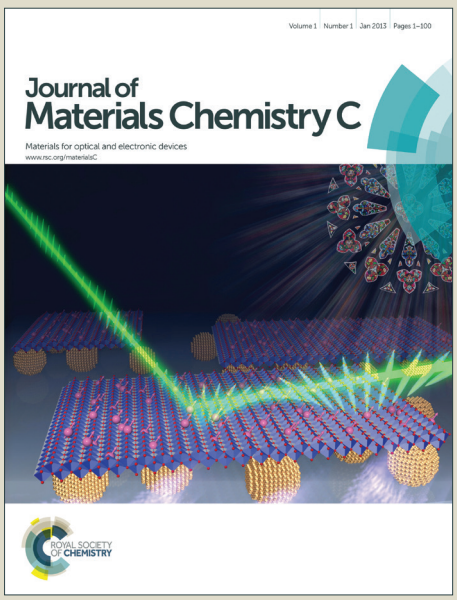

ROYAL SOCIETY OF CHEMISTRY

www.rsc.org/materialsC

Prediction of magnetic anisotropy of 5d transition-metal doped g-C_3N_4

Yun Zhang[1], Zhe Wang[1], Juexian Cao[1,2,*]

[1]*Department of Physics, Xiangtan University, Xiangtan, Hunan, 411105, China*

[2]*Beijing Computational Science Research Center, Beijing, 100084, China*

**Corresponding author. Tel.:+8618673210632. E-mail address: jxcao@xtu.edu.cn.*

Abstract:

Based on density functional theory, we investigated the magnetic properties of 5d transition metal (TM) atoms at porous sites of graphene-like carbon nitride (g-C_3N_4). Our results show that the TM adatoms bind to g-C_3N_4 much stronger than to graphene due its unique porous structure. The magnetic anisotropy energies (MAEs) for TM doped g-C_3N_4 are investigated by using torque method. Huge MAEs are obtained, especially for Ir@g-C_3N_4 12.4 meV/atom with an easy axis perpendicular to the plane. Moreover, the MAE can be enhanced to 56.9 meV/atom by applying electric field up to 1.0 V/ Å.

PACS numbers:

Keywords:

Due to the requirement of high density magnetic storage for information technology, much of the interest has concentrated on the question of minimization the size of magnetic domain for classical information storage. The key issue is to increase the magnetic anisotropy energy (MAE) per atom to inhibit magnetization reversal and hence loss of information [1]. It is well known that reduced symmetry and low-dimensionality would induce appreciable MAE. Heuristically thinking, the ultimate size of a record magnetic bit with large magnetic anisotropy originates from an isolated magnetic atom on a nonmagnetic substrate. Much attention has been paid to the magnetic properties of monoatomic chains, dimers and clusters and also the adatom on substrate [2-4]. Based on ab inito calculations, it is reported that giant values of MAE have been obtain for free-standing monoatomic wires, especially for 4d and 5d transition metal monowires [5]. Fernández performed spin density functional calculations and found that the isolated Pt dimer and Ir dimer provide large MAE with the order of 220 meV and 100 meV, respectively [4]. Free transition-metal cluster with 3-7 atoms were predicted to show large value of MAE according to tight-binding model calculations [6]. The MAE of metal cluster with gas phase is also investigated within frame of density functional calculations and the MAE of Ir_4 and Pt_4 are about 130 meV and 50 meV, respectively [4]. Unfortunately, such fascinating value of MAE can not survive when the monoatomic chains, dimers and clusters are incorporated into the substrate due to the quenchment of their spin

and orbital moment. Many efforts have been devoted to seek a suitable host for magnetic nanostructures. Xiao reported giant MAE of TM dimers on benzene and grapheme [7]. Zhang predicted that 5d transition metals on graphene present colossal MAE [8]. However, many studies demonstrated that TM adatoms on pristine graphene suffer the problem of instability [9-11]. One feasible way to bind TM atoms more firmly on graphene is to attach them to defects [12-15]. Very recently, it is found that TM dimers on a single vacancy or a nitrogen-decorated divacancy graphene are extremely stable and possess high MAE. This offers great opportunity for technological developments of robust magnetic nanostructures.

Inspired by the unique properties of graphene, carbon nitride (C_3N_4) has attracted increasing interest owing to its potential applications in catalyst, energy conversion and environmental protection [16-18]. C_3N_4 can exist in various allotropes with different the C to N ratio and the atomic arrangements. In general, the tri-s-triazine-based graphene-like carbon nitride (g-C_3N_4) is regarded to be the most energetically favorable structure [19]. The unique porous structure with well-ordered vacancies makes g-C_3N_4 a promising substrate for stable and uniformly dispersed adsorption of TM atoms due to the fact that each pore can only host one metal atom [20, 21].

In this study, we present our first-principles study on the structural stability and magnetic properties of 5d TM atom embedded in g-C_3N_4 monolayer. Total energy calculations show that the binding energy for TM

atoms to g-C3N4 is extremely strong. Most interestingly, huge MAE up to 12.8 meV/atom is found for Ir@g-C_3N_4. Moreover, the MAE is conveniently manipulated by applying electric field. Our results demonstrated that the MAE can reach to 56.9 meV/atom with electric field up to 1 V/Å.

The structure of 5d TM atom embedded in g-C_3N_4 was mimicked as a supercell composed of 2 × 2 g-C_3N_4 unit cells with one TM atom at porous site, as shown in Fig. 1. A series of 5d TM such as Ta, W, Re, Os and Ir are taken into our consideration. The vacuum thickness along the z axis was set to 15Å, which is large enough to avoid the interaction between adjacent layers. First-principles calculations were performed based on the density-functional theory (DFT) as implemented in the Vienna ab initio simulation package (VASP) [22, 23]. The exchange-correlation potential is treated with the Perdew-Burke-Eznerh of generalized-gradient approximation (PBE-GGA) [24]. We used the projector augmented wave (PAW) method for the description of the electron–ion interaction. A 15 × 15 Γ-centered k-point mesh was used to sample the Brillouin zone of the supercell. For geometry optimization, all the internal coordinates are fully relaxed until the Hellmann-Feynman forces are less than 0.01eV/ Å. The MAE is obtained by applying the torque approach which has been proved to be an effective method for the reliable determination of MAE [25,26]. Due to the strong SOC of 5d TM systems, we also used the direct method by including spin orbit coupling (SOC) to calculate the MAE to check the reliability of the torque approach,

with the non-collinear mode of the VASP. It is defined as MAE=E(x)-E(z). Here, E(x) and E(z) represents the total energy of self-consistent calculations in z and x magnetization directions, respectively. However the direct method is much more expensive than the torque method due to the need of extremely fine sampling meshes for the k-space integrations.

For the convenience of discussions, we remind that the contributions to MAE from the same spin, i.e. up-up ($\uparrow\uparrow$) or down-down ($\downarrow\downarrow$) within the second-order perturbation can be expressed as [27]:

$$MAE = (\xi)^2 \sum_{o,u} \frac{\left|\langle o | L_z | u \rangle\right|^2 - \left|\langle o | L_x | u \rangle\right|^2}{E_u - E_o} \qquad (1)$$

where o and u denote occupied and unoccupied electronic states. E_o and E_u are their band energies, respectively. L_z and L_x are the angular momentum operators. ξ is the strength of SOC. Note that the corresponding contributions to the MCA from different spin, i.e. up-down ($\uparrow\downarrow$) or down-up ($\downarrow\uparrow$) can be expressed as:

$$MAE = (\xi)^2 \sum_{o,u} \frac{\left|\langle o | L_x | u \rangle\right|^2 - \left|\langle o | L_z | u \rangle\right|^2}{E_u - E_o} \qquad (2).$$

Contributions from the d states, the nonzero matrix elements of the L_z and L_x operators are $\langle xz|L_z|yz\rangle=1$, $\langle x^2\text{-}y^2|L_z|xy\rangle=2$, $\langle xy|L_x|xz\rangle=1$, $\langle x^2\text{-}y^2|L_x|yz\rangle=1$ and $\langle z^2|L_x|xz,yz\rangle=\sqrt{3}$. It would be easy to find that the positive contribution to the MCA originates from two matrix elements of $\langle xz|L_z|yz\rangle$ and $\langle x^2\text{-}y^2|L_z|xy\rangle$, while $\langle xy|L_x|xz\rangle$, $\langle x^2\text{-}y^2|L_x|yz\rangle$ and $\langle z^2|L_x|xz,yz\rangle$ donate negative contribution, according to Eq. (1). However, contribution to MAE

from the nonzero matrix elements of the L_z and L_x operators are opposite in sign for different spin coupling, described in Eq. (2).

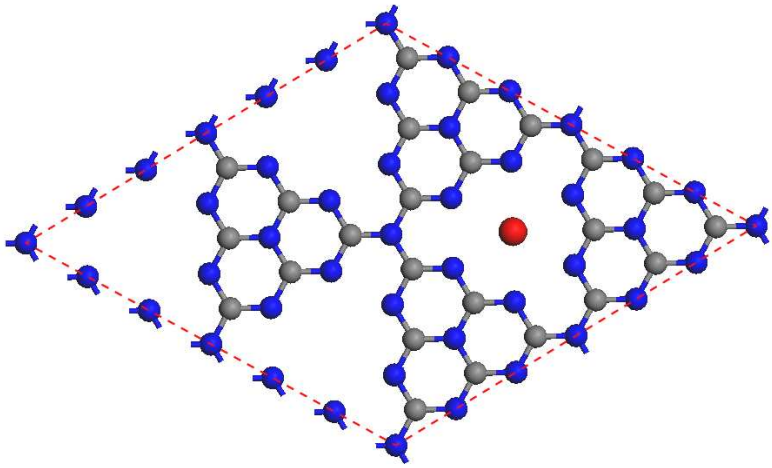

Fig. 1. Atomic arrangement of 5d TM atom embedded in 2×2 g-C_3N4. Gray, blue, and red balls denote as carbon, nitrogen, and metal atoms, respectively.

The calculated lattice constant of the unit cell for g-C_3N_4 monolayer is 7.135 Å, consistent with the previous studies [18]. The TM atoms were initially placed at the porous site of the g-C_3N_4 as shown in Fig. 1. After fully relaxation, we found that the metal atom almost remains in the plane of g-C_3N_4 sheet and the distortion of the g-C_3N_4 sheet could be negligible. This is reasonable because the vacancy in g-C_3N_4 sheet is large enough to host a metal atom. The bond length $d_{TM\text{-}N}$ is the distance between the TM dopant and its closest N atoms. The $d_{TM\text{-}N}$ as listed in Table I is in the range from 2.28 Å to 2.37 Å. The stability of TM atom on g-C_3N_4 are investigated through their binding energies, which is defined as $E_b = E(g\text{-}C_3N_4) + E(TM) - E(TM\ @\ g\text{-}C_3N_4)$. Here E(g-$C_3N_4$), E(TM), and

E(TM@g-C_3N_4) refers to the total energy of g-C_3N_4, TM atom, and the whole system consisting of TM and g-C_3N_4, respectively. In general, the binding energy decrease with the increasing of atomic number as listed in Table 1. This is because of the decreasing in the atomic radius with increasing the atomic number. Obviously, one can easily find that the Ta atom strongly binds to g-C_3N_4 with binding energy of 7.70eV while the Ir doping causes the weakest linkage. However, the binding energy is much larger than that of the TM on graphene [28]. Our calculation shown that all systems are magnetic: the largest local spin moment (M_s) of 1.75 μ_B is found for Ir in Ir@g-C_3N_4, while the smallest local M_s is 0.04 μ_B for Re in Re@ g-C_3N_4. To illustrate their magnetic states, we plot the spin densities of TM@g-C_3N_4 (TM=Ta, W, Os and Ir) in Figure 2. It can be clearly seen that the magnetism is predominantly around the central TM atoms. The moments of TM atoms are associated with strongly hybridized with their nearest neighbor C/N atoms.

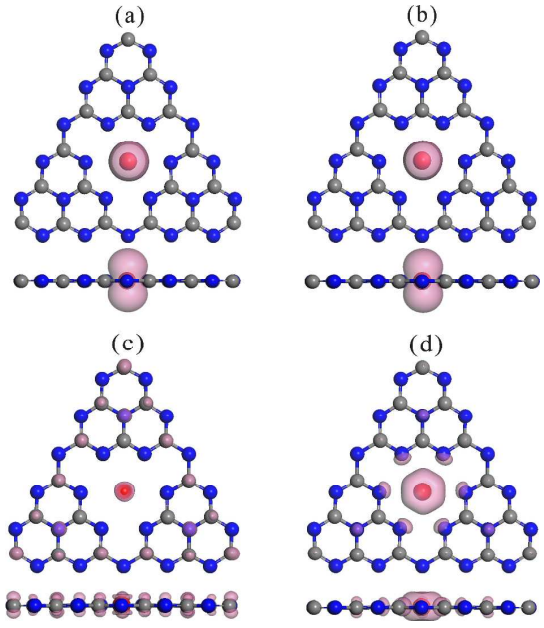

Fig. 2. Isosurfaces of the spin density (0.05 e/Å^3) of TM@g-C_3N_4 (TM=Ta, W, Os and Ir). Not show Re@g-C_3N_4 due to its small local M_s.

Table I. Binding energies (E_b in eV), bond length (d_{TM-N} in Å), and local spin magnetic moments of TM atom (M_s in μ_B) of metal doping g-C_3N_4.

System	Eabs(eV)	d_{TM-N} (Å)	Ms(μ_B)
Ta	7.70	2.32	1.59
W	6.17	2.30	1.61
Re	3.65	2.28	0.04
Os	3.72	2.29	0.15
Ir	3.02	2.37	1.75

The calculated MAEs with both the torque and direct methods are plotted in Fig. 3. The two approaches produce almost the same MAEs for all cases [29]. The important finding here is that 5d TM@g-C_3N_4 have sizable MAE except Re@g-C_3N_4. In particular, we found that the MAE for Ir@g-C_3N_4 is 12.4 meV, with an easy axis perpendicular to the plane of g-C_3N_4 sheet. Similar to Ir@g-C_3N_4, Ta@g-C_3N_4 and W@g-C_3N_4 possesses considerable perpendicular MAE of 10.0 meV and 10.3 meV, respectively. The MAE for Os@g-C_3N_4 is 12.2 meV while the easy axis is in the plane of g-C_3N_4 sheet.

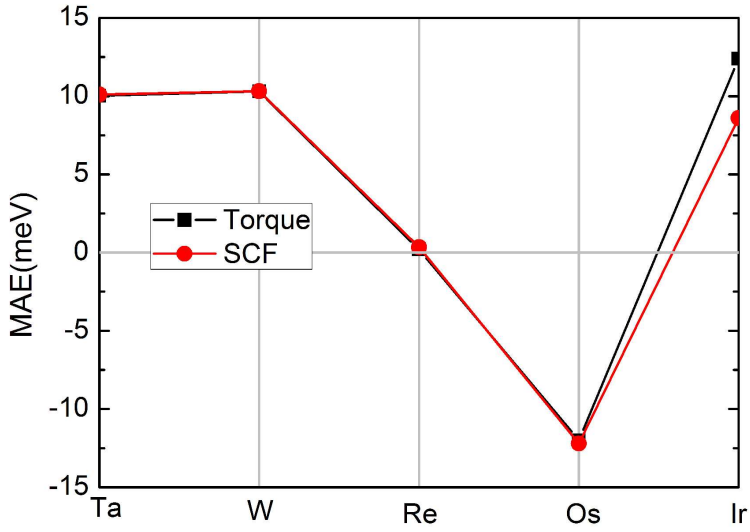

Fig. 3. MAEs of the 5d TM@g-C_3N_4. Both the torque method and the total energy of self-consistent calculations (SCF) with SOC were used to calculate the MAEs. Positive and negative signs of MAE correspond to out-of-plane (perpendicular) and in-plane easy axes, respectively.

To understand the origin of MAE in electronic structure, we present the projected density of states (PDOS) of different d orbitals of TM@g-C_3N_4 (TM=Ta, W, Re, Os and Ir) in Fig. 4(a)-(e). According to Eq. (1) and Eq. (2), we can reveal the driving factor of the MCA. For the case of Ta@g-C_3N_4, as seen in Fig. 4(a), matrix elements of angular momentum operator L_z between majority-spin occupied $d_{xz/yz}$ and unoccupied $d_{xz/yz}$ provide the primary contribution to the positive MAE. The negative contribution from matrix elements of L_z between minority-spin occupied $d_{xz/yz}$ and majority-spin unoccupied $d_{xz/yz}$ is cancelled out by positive contribution from matrix elements of L_x between majority-spin occupied $d_{xz/yz}$ and minority-spin unoccupied d_{z^2}. Thus Ta@g-C_3N_4 possesses a perpendicular MAE of 10.0 meV. We obtained a large positive MAE of 10.3 meV for W@g-C_3N_4.

In Fig. 4(b), the negative contribution from matrix elements of L_z between minority-spin occupied $d_{xz/yz}$ and majority-spin unoccupied $d_{xz/yz}$ is totally compensated by positive contribution from matrix elements of L_x between majority-spin occupied $d_{xz/yz}$ and minority-spin unoccupied d_{z^2}. Therefore, there is a net positive contribution due to a smaller energy separation between $d_{xz/yz}$ and d_{z^2}, since it provides a sufficiently small denominator in Eq. (1). As shown in Fig. 4(c), for Re@g-C_3N_4, there is only few majority-spin occupied $d_{xz/yz}$ near the Fermi level. The positive contribution from matrix elements of L_z between majority-spin occupied and unoccupied $d_{xz/yz}$ is nearly compensated by the negative contribution from matrix elements of L_z between majority-spin occupied and minority-spin unoccupied $d_{xz/yz}$. Consequently, the net positive contribution is 0.34 meV. For Os@g-C_3N_4, there are majority-spin occupied and minority-spin unoccupied $d_{xz/yz}$ just around the Fermi level, as shown in Fig. 4(d). These states contribute to the in-plane MCA through matrix elements of $\left\langle d^u_{xz/yz} \middle| L_x \middle| d^o_{xz/yz} \right\rangle$. Ir@g-$C_3N_4$ renders the most appreciable MAE. We identified that the couplings between majority-spin occupied d_{xy/x^2-y^2} and minority-spin unoccupied $d_{xz/yz}$, through $\left\langle d^u_{xy/x^2-y^2} \middle| L_x \middle| d^o_{xz/yz} \right\rangle$, play the dominant role for the giant positive MAE of Ir@g-C_3N_4.

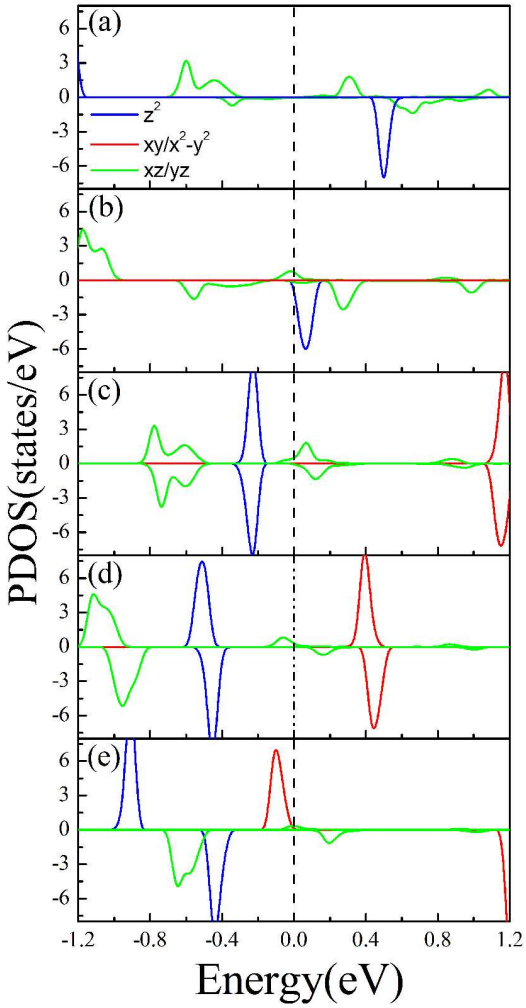

Fig. 4. (a)-(e) The calculated projected density of states (PDOS) of the d orbitals of TM@g-C_3N_4 (TM=Ta, W, Re, Os and Ir).

Nevertheless, it is of practical interest to manipulate the magnetic anisotropy. Within the rigid band model, which can predict the MAE against the shift of the Fermi level, we calculated MAE as a function of the position of the Fermi level. As shown in Fig. 5, the MAE of Ta@g-C_3N_4 is hardly changed if one shifts the Fermi level upwards or downwards within a range of -0.2—0.2eV. For W@g-C_3N_4, the MAE is even negative if one shifts the Fermi level upwards by 0.1eV. It is interesting that the MAE of Ir@g-C_3N_4 rapidly increases when the E_F shifts downwards. This gives us an easy way to manipulate the MAE by

applying an electric field (ε). To illustrate this idea, we included a moderate electric field (ε) in the self-consistent calculations and obtained the ε-dependence of MAE for Ir@g-C_3N_4. The direction of electric field is perpendicular to g-C_3N_4 plane. As shown in Figure 6(a), the presence of an electric field significantly increases the MAE of Ir@g-C_3N_4, with a large slope of 45.2 meV per V/ Å, which proves the speculation from the rigid band model well. It is noticeable that MAE can be enhanced to 56.9 meV at ε=1V/ Å.

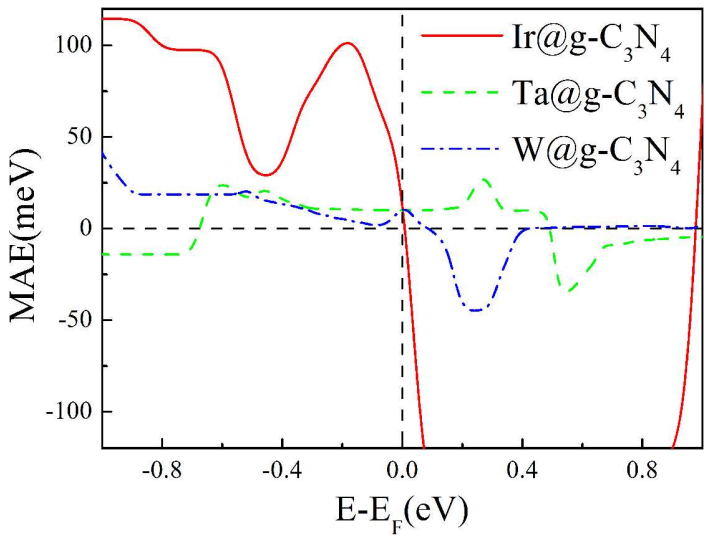

Fig. 4. Fermi level dependent total MAE for Ta@g-C_3N_4, W@g-C_3N_4 and Ir@g-C_3N_4 from torque method with rigid band model, respectively. The vertical dashed lines mark the real Fermi level (E_F).

To find out the driving factor of the giant variation, we investigate the PDOS of Ir@g-C_3N_4 at ε=0V/Å and ε=1V/Å, as presented in Fig. 6(b) and (c). One can note that the electric field cause major effects: (1) the majority-spin occupied d_{xy/x^2-y^2} states below the Fermi level now become empty, along with

(2) the minority-spin occupied $d_{xz/yz}$ and d_{z^2} states are pushed to higher energy states. Compared to ε=0V/Å case, the positive contribution from $\left\langle d^{u}_{xz/yz} \left| L_x \right| d^{o}_{xy/x^2-y^2} \right\rangle$ is increased due to the more $d_{xz/yz}$ near the Fermi level.

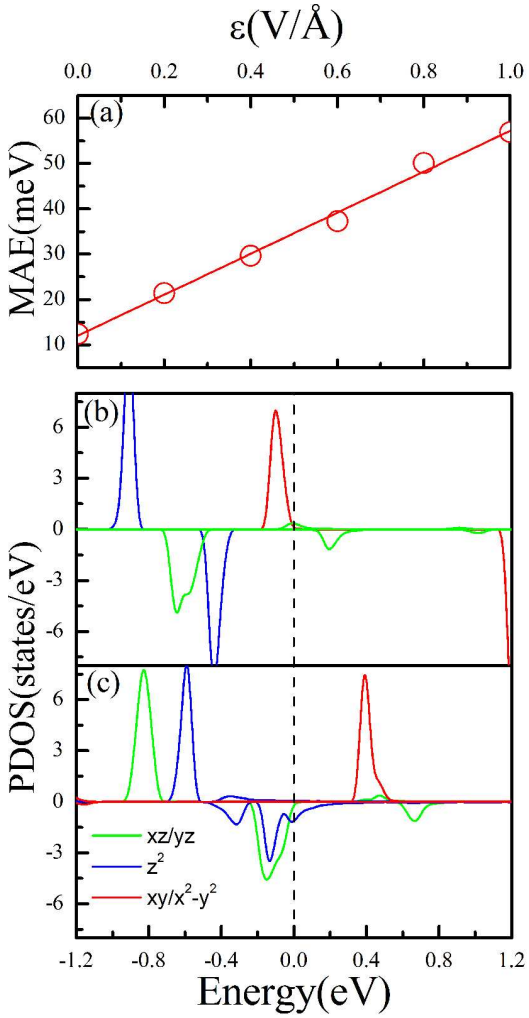

Fig. 5. (a) Total MAE of Ir@g-C_3N_4 under electric field (ε) from 0 to 1.0 V/Å. (b) and (c) The calculated PDOS of the d orbitals of Ir@g-C_3N_4 for ε=0V/ Å and ε=1V/ Å, respectively.

To summarize, we reported a systematic DFT study of the geometry structure, binding energy, spin moments and MAE of 5d TM@g-C_3N_4 systems. We found that 5d TM binding energies are much stronger on g-C_3N_4 than on graphene. Intriguingly, a large MAE is predicted for Ir@g-C_3N_4. Furthermore,

using the rigid band model analysis, we propose that the MAE of Ir@g-C_3N_4 can be tuned by applying a moderate electric field. Our present study identifies g-C_3N_4 as an excellent template for TM atom adsorption.

ACKNOWLEDGMENTS

The authors are grateful to Jun Hu for fruitful discussions. This work is supported by National Natural Science Foundation of China (No.11074212, 11204259, 11374252), the Program for New Century Excellent Talents in University (Grant No. NCET-12-0722) and Changjiang Scholars and Innovative ResearchTeam in University (Grant No. IRT1080).

References:

1. P. Gambardella, S. Rusponi, M. Veronese, S. S. Dhesi, C. Grazioli, A. Dallmeyer, I. Cabria, R. Zeller, P. H. Dederichs, K. Kern, C. Carbone, and H. Brune, Science 300, 1130 (2003).
2. T. O. Strandberg, C. M. Canali, and A. H. MacDonald, Nature Mater. 6, 648 (2007).
3. P. Błoński and J. Hafner, Phys. Rev. B 79, 224418 (2009).
4. L. Fernández-Seivane and J. Ferrer, Phys. Rev. Lett. 99, 183401 (2007).
5. Y. Mokrousov, G. Bihlmayer, S. Heinze, and S. Blügel, Phys. Rev. Lett. 96, 147201 (2006).
6. G.M. Pastor, J. Dorantes-Dávila, S. Pick, and H. Dreyssé, Phys. Rev. Lett. 75, 326 (1995).
7. R. J. Xiao, D. Fritsch, M. D. Kuz'min, K. Koepernik, H. Eschrig, M. Richter, K. Vietze, and G. Seifert, Phys.Rev.Lett. 103, 187201 (2009).
8. H. Zhang, C. Lazo, S. Blügel, S. Heinze, and Y. Mokrousov, Phys. Rev. Lett. 108, 056802 (2012).
9. R. Varns and P. Strange, J. Phys.: Condens. Matter 20, 225005 (2008).
10. Y. Sanchez-Paisal, D. Sanchez-Portal, and A. Ayuela, Phys.Rev.B 80, 045428 (2009).
11. K. T. Chan, J. B. Neaton, andM. L. Cohen, Phys.Rev.B 77, 235430 (2008).
12. A. V. Krasheninnikov, P. O. Lehtinen, A. S. Foster, P. Pyykkö, and R. M. Nieminen, Phys. Rev. Lett. 102, 126807 (2009).
13. S. Kattel, P. Atanassov, and B. Kiefer, J. Phys. Chem. C 116, 8161−8166, (2012).
14. J. A. Rodriguez-Manzo, O. Cretu, and F. Banhart, ACS Nano 4, 3422 (2010).
15. J. Hu, R. Wu, Nano Lett. 14 , 1853 (2014).
16. Y. Zheng, J. Liu, J. Liang, M. Jaroniec and S. Z. Qiao, Energy Environ. Sci. 5, 6717 (2012).
17. M. Wu, Q. Wang, Q. Sun, and P. Jena, J. Phys. Chem. C 117, 6055 (2013).

18. Q. Liu, and J. Zhang, Langmuir 29, 3821 (2013).
19. E. Kroke,M. Schwarz, E. Horath-Bordon, P. Kroll, B. Noll and A. D. Norman, New J. Chem. 26, 508 (2002).
20. H. Pan, Y. W. Zhang, V. B. Shenoy, H. Gao. Nanoscale Res. Lett. 6, 97 (2011).
21. X. Wang, X. Chen, A. Thomas, X. Fu, M. Antonietti, Adv. Mater. 21, 1609 (2009).
22. G. Kresse and J. Hafner, Phys. Rev. B 48, 13115 (1993).
23. G. Kresse and J. Furthmuller, Phys. Rev. B 54, 11169 (1996).
24. J. P. Perdew, K. Burke and M. Ernzerhof, Phys. Rev. Lett. 77, 3865 (1996)
25. X. Wang, R. Wu, D. S. Wang and A. J. Freeman, Phys. Rev. B 54, 61 (1996).
26. J. Hu, R. Wu, Phys. Rev. Lett. 110, 097202 (2013).
27. D. S. Wang, R. Q. Wu, and A. J. Freeman, Phys. Rev. B 47, 14932 (1993).
28. V. Zólyomi, Á. Rusznyák, J. Kürti, and C. J. Lambert, J. Phys. Chem. C 114, 18548 (2010).
29. J. Hu, R. Wu, arXiv, 1402.0278 (2014).